Theoretical study of possible active site structures in Cobalt-Polypyrrole catalysts for oxygen reduction reaction

Shi, Zheng; Liu, Hansan; Lee, Kunchan; Dy, Eben; Chlistunoff, Jerzy; Blair, Michael; Zelenay, Piotr; Zhang, Jiujun; Liu, Zhong-Sheng

Publisher's version / Version de l'éditeur:
https://doi.org/10.1021/jp2027719
The Journal of Physical Chemistry C, 115, 33, pp. 16672-16680, 2011-07-14

THE JOURNAL OF PHYSICAL CHEMISTRY C

ARTICLE

pubs.acs.org/JPCC

Theoretical Study of Possible Active Site Structures in Cobalt- Polypyrrole Catalysts for Oxygen Reduction Reaction

Zheng Shi,[*,†] Hansan Liu,[†,§] Kunchan Lee,[†,∥] Eben Dy,[†] Jerzy Chlistunoff,[‡] Michael Blair,[‡] Piotr Zelenay,[‡] Jiujun Zhang,[†] and Zhong-Sheng Liu[†]

[†]NRC-Institute for Fuel Cell Innovation, 4250 Wesbrook Mall, Vancouver, British Columbia, Canada

[‡]Los Alamos National Laboratory, Los Alamos, New Mexico 87545, United States

ABSTRACT: The active site structure of nonprecious group metal catalyst is a puzzle which inhibits innovative synthetic route design and impedes breakthroughs. In an effort to understand the origin of the catalytic activity of Co-PPy composites, we employed density functional theory (DFT) and experimental measurements to investigate the structure and energy of possible catalytic sites and the corresponding reaction pathways for the oxygen reduction reaction (ORR). Four different structures of the active site are examined, including two previously postulated in the literature. In order to determine the probability of their existence, the stability of each structure is evaluated. The corresponding Co(III)/Co(II) redox potentials are calculated and, based on the obtained data, the involvement of either Co(III) or Co(II) in the ORR under fuel cell-relevant conditions postulated. Possible configurations of oxygen adsorption on the active centers are also examined, including the end-on and side-on cases. The possible reaction pathways and reaction products generated at the various active centers are evaluated based on Yeager's concept correlating ORR products with the configuration of oxygen adsorption. The catalytic activity is found to be significantly different for the various sites and depends strongly on the electrode potential. The computational data are critically compared with experimental spectroscopic (EXAFS and FTIR) and electrochemical data (CV, RDE, and RRDE). The insights into the active structures and their associated catalytic activity as well as selectivity for four-electron oxygen reduction are expected to provide guidance for further catalyst optimization.

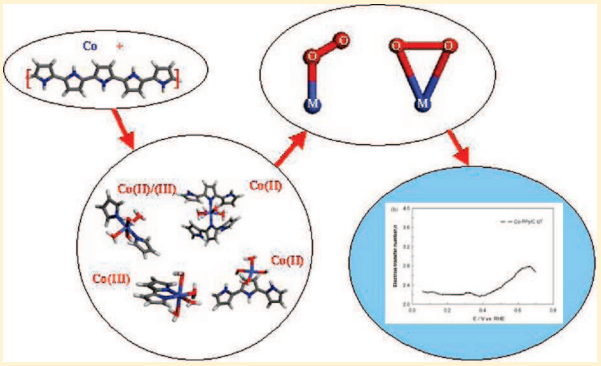

INTRODUCTION

Growing energy and environmental challenges facing the world today have made fuel cell research, particularly the development of nonprecious group metal (non-PGM) catalyst for oxygen reduction reaction (ORR) an important area of energy-related research.[1] Fuel cells, the polymer electrolyte membrane fuel cell (PEMFC) in particular, represent a promising technology that is capable of generating energy in a clean and sustainable way. In the past two decades or so, significant research effort has been focused on reducing the barriers for fuel cell commercialization, such as the high cost, limited durability, and unsatisfactory performance. The use of Pt in the PEMFC catalysts, mainly those for the cathode, limits the fuel cell performance and contributes to the high fuel cell cost. (The price of Pt increased from $443/troy ounce in January 2000 to $1789/troy ounce in January 2011, reaching as much as $2,280/troy ounce at its maximum in March 2008).[2] The limited abundance in the earth crust likely deems Pt unsustainable for mass use in high-power fuel cell systems. Furthermore, poor stability of Pt under the operating conditions of the fuel cell cathode negatively impacts the PEMFC durability. Thus, the development of non-Pt catalysts is likely to be required for the large-scale commercialization of fuel cell systems.

In the past decade, significant progress has been achieved in the catalytic activity and durability of nonprecious group metal catalysts derived from transition metals, nitrogen and carbon.[3,4] Recently, the non-PGM catalytst synthesized with Fe and cyanamide has demonstrated an open cell voltage (OCV) of 1.04 V and current densities of 165 A cm^{-3} at 0.80 V,[5] allowed to meet the 2010 US DOE target for the volumetric ORR activity of non-PGM catalysts (130 A cm^{-3} at 0.80 V).[6] These encouraging results will likely fuel further non-PGM catalyst research.

In spite of progress in non-PGM catalysts to date, there are some fundamental challenges that impede the improvement in mass activity of the catalysts, inhibit innovative synthetic route design, and impede breakthroughs. These challenges are primarily associated with the nature, structure and ORR mechanism at heat-treated catalysts. While the heat treatment enhances the catalyst activity and stability it also makes the active-site identification extremely difficult, if at all possible. Consequently, further increase in the active-site density and mass activity of

Received: March 24, 2011
Revised: May 27, 2011
Published: July 14, 2011

non-PGM catalysts is difficult as is the design of alternative and innovative routes for new catalyst synthesis.

Much effort has been devoted to gaining knowledge of the nature and structure of active ORR site(s) in non-PGM catalysts.[7−25] The likely active-site structures have been summarized by Dodelet in a 2006 review of non-PGM catalyst litereature.[1] The sites include the following most frequently considered ones: (a) M-N_4 site, similar to the one proposed for metal macrocycles by van Veen et al.;[10] (b) M-N_x sites, first proposed by Yeager and co-workers,[7,8] and further developed by the Dodelet group, and others;[1] and (c) metal-free carbon structure, as originally proposed by Wiesener[11] (with metal serving merely as a catalyst for the ORR active-site formation).

The debate about whether or not the transition metal is a part of the catalytic site is at the center of active-site discussion in the non-PGM catalyst research community.[23,26] A number of theoretical studies were carried out in order to simulate various catalytic sites with[27−30] and without the metal.[31,32] The results indicate that catalytic sites with and without a transition metal could catalyze a four-electron ORR.

In order to understand non-PGM catalyst active-site structure and reaction mechanism, electrochemical studies of cobalt polypyrrole (Co-PPy) catalyst systems with and without the heat treatment have been carried out.[3,33−35] The studies demonstrated that even without the heat treatment, Co-PPy exhibits ORR activity. In the case of a non-heat-treated Co-PPy, rotating ring-disk electrode (RRDE) data yielded an average number of electrons transferred per O_2 molecule in the reaction of 2.2 at 0.3 V (vs RHE). That number increased to 3.1 after the heat treatment. The study also showed that the number of electrons transferred is a function of electrode potential. For untreated Co-PPy catalysts, the number rose to 2.8 when the electrode potential was increased to 0.6 V (vs RHE), however, the number decreased to about 2.6 for heat treated catalysts at the same potential.[35] Thus, at this potential, the electron transfer number with heat-treated catalyst is less than that without heat treatment. An X-ray photoelectron spectroscopy (XPS) study indicated the existence of two types of nitrogen in untreated Co-PPy catalysts giving rise to N 1s peaks at 398.5 and 399.9 eV, respectively.[35] The first peak was assigned to the Co−N binding and the second to the N−H binding in pyrrole. Since it was demonstrated that pyrrole could not catalyze ORR, the catalytic activity of untreated Co-PPy can be attributed to Co−N sites with some probability. Two types of active-site structures were postulated in the literature: one involving cobalt coordinated by four nitrogens[34] and the other with only two nitrogens.[3]

In an effort to better understand the performance of Co-PPy catalysts, we employed density functional theory (DFT) for exploring the active-site structures and ORR mechanism in non-heat-treated Co-PPy. We focused on several types of active-site structures. We first studied their structure properties and these properties are compared with available experimental structure data, such as FTIR, XRD, and EXAFS. We further examined the stability of these structures. With the modified and validated redox potential calculation method, we evaluated the redox potential for different structures to understand their contribution to ORR activity at various potentials. We also investigated possible oxygen adsorption configurations to understand reaction pathways and products. The results of this theoretical study were then critically compared with electrochemical data, including the experimentally observed dependence of ORR activity and selectivity on potential. The insights into the active structures and their associated catalytic activity as well as selectivity for four-electron oxygen reduction are expected to provide guidance for further catalyst optimization.

COMPUTATIONAL METHODS

In this work, we used Materials Studio DMol3 (version 4.0) program from Accelrys[36,37] to carry out DFT calculations with Vosko−Wilk−Nusair[38] local correlation functional, and Becke[39] and Perdew−Wang[40] (VWN-BP) no local correlation functional. An effective potential with relativistic effect accounted DFT semicore pseudopotential was applied for the cobalt atom. Double numerical plus (DNP) polarization function basis sets were employed in the calculations. The spin-unrestricted method was used for all open-shell systems. The geometry convergence thresholds for energy change, max force, and max displacement were 0.00002 hartree, 0.004 hartree/Å, and 0.005 Å, respectively. Our previous studies of the transition metal macrocycle systems have demonstrated that the computational methodology provides satisfying geometric structures and electronic properties, such as ionization potential and oxygen binding energies for this type of system.[41]

We utilized a modified version of the approach proposed by Nørskov et al.[42,43] in reversible potential calculation. In our interpretation, the reversible potential of an electron transfer reaction in acidic solution,

$$A + H^+ + e^- \rightarrow AH \quad (1)$$

can be calculated with reference to the proton reduction reaction in acidic solution,

$$H^+ + e^- \rightarrow 1/2H_2 \quad (2)$$

Thus, thermochemical calculation of the electrochemical reaction 1 referenced to the standard hydrogen electrode can be simplified as a calculation of a chemical reaction 3 obtained by subtracting reaction 2 from reaction 1,

$$A + \frac{1}{2}H_2 \rightarrow AH \quad (3)$$

The result is interpreted as the electrochemical potential of reaction 1 versus the standard hydrogen electrode potential.

While the resulting reaction 3 is the same as that proposed by Nørskov et al., the interpretation of this reaction is different. In the calculation of free energy change, $\Delta G_0 = \Delta E + \Delta ZPE + T\Delta S$, ΔE is the electronic energy change term, ΔZPE is the zero point energy correction term and $T\Delta S$ is the entropy change term. Nørskov et al. took $T\Delta S$ values from standard tables for molecules in the gas phase and used a first principle theoretical method to obtain ΔE and ΔZPE terms. In our approach, we omitted the $T\Delta S$ term because of the complexity and low accuracy of the entropy calculations for nongaseous systems. Instead, an empirical correction was introduced to the calculated standard potentials, based on the correlation between the accurately determined experimental[44] and the calculated standard potentials for a number of relevant redox systems:

$$O_2 + H^+ + e^- \leftrightarrow HO_2 \quad (4)$$

$$HO_2 + H^+ + e^- \leftrightarrow H_2O_2 \quad (5)$$

$$HO_2 + H^+ + e^- \leftrightarrow O + H_2O \quad (6)$$

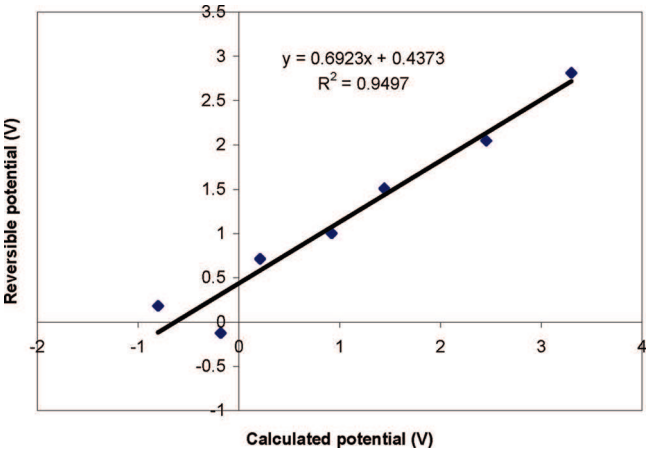

Figure 1. The relationship between experimental reversible potentials and calculated reversible potentials.

$$H_2O_2 + H^+ + e^- \leftrightarrow HO + H_2O \quad (7)$$

$$O + H^+ + e^- \leftrightarrow OH \quad (8)$$

$$HO + H^+ + e^- \leftrightarrow H_2O \quad (9)$$

$$Co(OH)_3 + H^+ + e^- \leftrightarrow Co(OH)_2 + H_2O \quad (10)$$

The computational results are compared with the experimental data in Figure 1. The experimental reversible potentials were taken from the book "Standard Potentials in Aqueous Solutions".[44] For reaction 10, the experimental number was obtained by correcting the redox potential in the alkaline solution (pH effect) using Nernst equation.[44] The figure clearly demonstrates that there is a good correlation between the experimental and computed reversible potential values. In the remaining part of the work, all calculated reversible potentials are corrected using the relationship shown in Figure 1.

■ ACTIVE-SITE STRUCTURE MODELS

In the literature, there are two postulated ORR active-site structures for Co-PPy catalysts: a four-N coordinated structure by Yuasa et al.[34] (Scheme 1a) and the two-N coordinated structure by Bashyam and Zelenay[3] (Scheme 1b).

A previous XPS study showed the existence of Co−N in non-heat-treated Co-PPy catalyst. Amorphous Co was also detected by electron paramagnetic resonance (EPR) spectroscopy in such non-heat-treated Co-PPy catalysts as indicated by the broad resonance near $g = 2$ in Figure 2a.[45] After activation by the heat treatment (Figure 2b), the EPR signal changes dramatically. The narrow isotropic, resonance (as opposed to the broad, axially symmetric resonance of Figure 2a) is clearly not consistent with amorphous Co, and the resonance is also not consistent with EPR signals detected from PPy, carbon, or Nafion. In addition, the temperature dependence in Figure 2b, where the signal intensity initially decreases and then increases with decreasing temperature suggests that the signal is due to isolated metal sites, most likely Co^{2+} ions.[46,47] Furthermore, the absence of hyperfine splitting implies that the ions have been incorporated into a network structure, such as a carbon ring that does not contain nuclei with nonzero spins. Another FTIR study of Co-PPy catalysts

Scheme 1. Active-Site Structures Postulated in the Literature: (a) N_4 Coordination Proposed by Yuasa et al.;[33] (b) N_2 Coordination Proposed by Bashyam and Zelenay.[3]

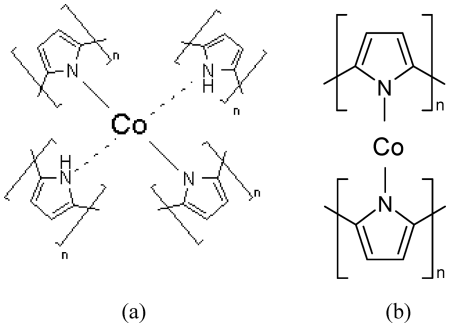

revealed the presence of a band near 1100 cm^{-1}, assigned to Co−N vibrational mode.[48]

In order to explore other possible structures, we also searched crystal structures containing cobalt and pyrrole. Below, we present the results of the study involving four possible structures as shown in Figure 3 and elaborated on in the following sections. These structures are as follows:

(a) Type A: two-N, two-polypyrrole-chains coordinated structure proposed by Bashyam and Zelenay;[3]
(b) Type B: two-N, one-polypyrrole-chain coordinated structure; similar to $M-N_2$ structure proposed in the literature;[1]
(c) Type C: π-coordinated structures, observed in crystals containing cobalt and pyrrole;[49]
(d) Type D: four-N and four-polypyrrole-chain coordinated structure proposed by Yuasa et al.[34]

The structures in Figure 3 illustrate different types of bonding between Co and polypyrrole. In addition, as cobalt is a transition metal, it will generally form coordination complexes. So for the active site structure, besides polypyrrole, water ligands are coordinated with cobalt. Moreover, six-coordination structure is employed in this work as the report showed that six-coordination distorted octahedral structure is a preferred coordination structure for cobalt polypyrrole.[50]

■ RESULTS AND DISCUSSION

Structure Study. With DFT methodology presented in the Computational section, we optimized all active site model structures. The results are presented and discussed in this section. Furthermore, we compared the computational results with available experimental data and discussed the likelihood of each structure in the cobalt polypyrrole composites.

For structure D1 (Figure 4), it is clear that Co can form two strong bonds with the negatively charged pyrrolic nitrogens (R_{Co-N} = 1.88 Å) but not with the neutral, protonated pyrrolic nitrogen (R_{Co-N} = 5.86 Å). Furthermore, unlike the porphyrin systems, in which the electrons are delocalized over the aromatic rings and the structure is planar, polypyrrole has a nonplanar gauche structure, with a torsional angle between two neighboring rings (<NCCN) of about 30° (a planar structure would have a torsional angle of 180°).[51] Co-PPy has a nonplanar structure as well. As illustrated in Figure 5, even with the smallest single pyrrole units, the structure A1 is nonplanar. Therefore, the formation of four nitrogen-coordinated Co structures associated with four polypyrrole chains, as proposed in the literature,[34] is

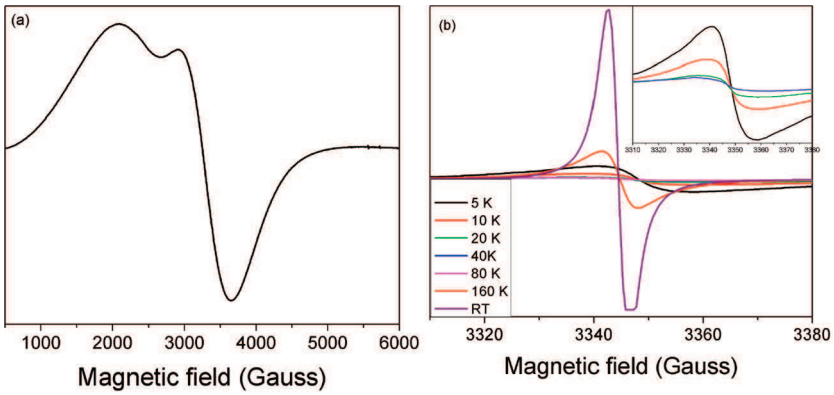

Figure 2. Electron paramagnetic resonance spectroscopy of Co-PPy catalysts: (a) unactivated, (b) temperature dependence of activated catalysts.

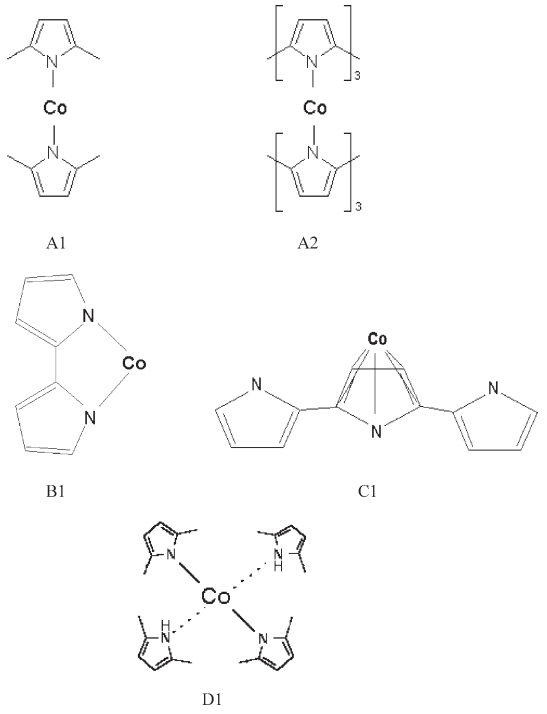

Figure 3. Active-site structure models.

unlikely. One can bring two arguments in favor of this conclusion: first, the neutral pyrrolic nitrogen forms a weak bond to Co; second, due to a steric hindrance, Co can only accommodate two polypyrrole chains, as seen in Figure 4. As a result, the optimized structure of D1 is very similar to structure type A in the sense that in both cases, Co is bonded to two nitrogens. Thus, in the following discussion, we will no longer separately consider the type D structure, as it is not sufficiently distinguishable from the type A structure. The optimized structures of the remaining three models are depicted in Figure 5; the bond distances for these structures are given in Table 1.

Experimental evaluation of catalyst structures has been conducted by X-ray diffraction (XRD) and extended X-ray absorption fine structure (EXAFS) spectroscopy. In particular, it was shown that mononuclear Co has the nearest N/O shell at a distance of 2.07 Å.[52] For the purpose of comparing with the available experimental data, we calculated averaged distances

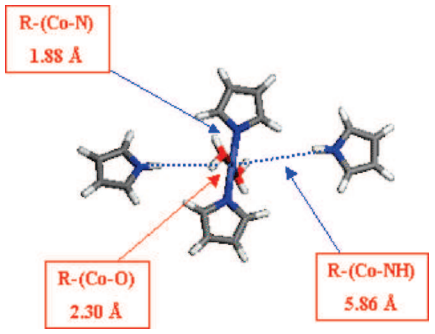

Figure 4. Optimized structure of D1. (Color: light blue − Co; dark blue − N; red − O; gray − C; white − H.).

between cobalt and nitrogen (R_{Co-N}) and between cobalt and oxygen (R_{Co-O}) in the first shell (Table 1). We then obtained the average Co−N/O distance ($R_{Co-N/O}$) from the following expression:

$$R_{Co-N/O} = \frac{N_{Co-N}R_{Co-N} + N_{Co-O}R_{Co-O}}{N_{Co-N} + N_{Co-O}} \quad (11)$$

where N_{Co-X} (X = N or O) is the number of Co−X bonds in the first shell. Strikingly, the calculated average distance ($R_{Co-N/O}$) of the model structures is exactly 2.07 Å, i.e., the experimentally measured value.[52]

Another available experimental structure information is the FTIR spectra of Co-PPy on carbon support (C-PPy-Co) recently reported by Martinez et al.[48] The spectra showed increased adsorption at 1116 cm^{-1} compared to the spectra of C-PPy (polypyrrole on C support without Co). To investigate the significance of the peak at 1116 cm^{-1}, we performed DFT calculations with Gaussian09.[53] We report our results obtained using the LanL2DZ[54−57] basis set and B3LYP[58] functionals. The calculations were also verified using other basis sets [6-31++G(d,p)] and exchange-correlation functionals [BLYP and BPW91]. An increase in IR adsorption for a peak centered at 1071 cm^{-1} (without frequency correction) was predicted for the A1 structure, whereas for the B1 structure a similar increase was predicted for a peak at 1048 cm^{-1} (without frequency correction). These increases in adsorption are due to new modes of in-plane vibration involving the two pyrroles bonded to Co as shown in Figure 6. The C1 structure does not give rise to an extra peak in the 1116 cm^{-1} (± 10%) region. The experimental frequency is

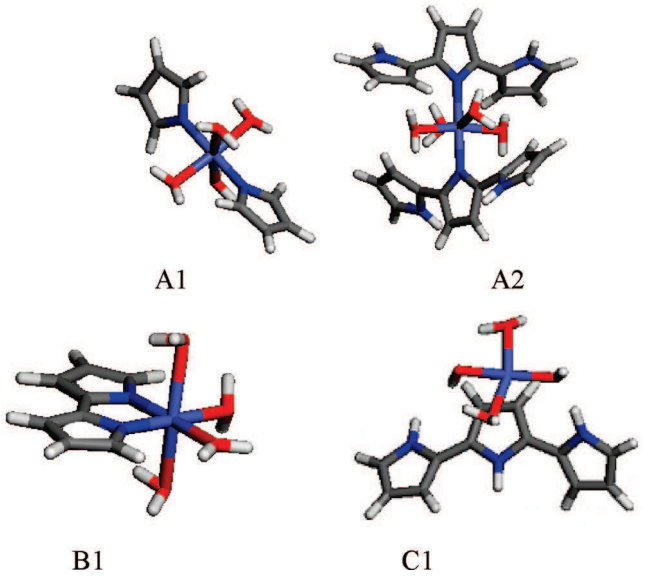

Figure 5. Optimized structures of A1, A2, B1, and C1. (Color: light blue − Co; dark blue − N; red − O; gray − C; white − H.).

slightly higher than that calculated, an expected difference as the pyrrole groups in the real catalyst are likely more rigid due to the bonding to the rest of the polymer chain. The presence of additional H_2O ligands around the Co center can also cause a blue shift. In brief, the DFT analysis of infrared spectra reported by Martinez et al.[48] strongly indicates the presence of the A and/or B type structures in Co-PPy catalysts. This, however, does not rule out the presence of C-type structures, since such structures are not expected to significantly alter the infrared spectra.

Stability Study. In order to estimate the stability of the model structures in the solution, we calculated their relative energies of formation from hydrated cobalt ions and polypyrrole as shown in eqs 12 to 14. For an exothermic reaction (a negative heat value), the calculations point to the cobalt-polypyrrole structure being energetically more favorable than the structure involving hydrated cobalt ions.

$$[Co(H_2O)_6]^{2+} + 2H\text{-}PPy_n + 4/3(H_2O)_3 \rightarrow PPy_n\text{-}Co\text{-}PPy_n(H_2O)_4 + 2[H(H_2O)_3]^+ \quad (12)$$

$$[Co(H_2O)_6]^{2+} + H_2\text{-}PPy_n + 4/3(H_2O)_3 \rightarrow Co\text{-}PPy_n(H_2O)_4 + 2[H(H_2O)_3]^+ \quad (13)$$

$$[Co(H_2O)_6]^{2+} + H\text{-}PPy_n + 4/3(H_2O)_3 \rightarrow [Co\text{-}HPPy_n(H_2O)_2(OH)_2] + 2[H(H_2O)_3]^+ \quad (14)$$

The calculated results are listed in Table 2. All reactions have negative ΔE values indicating that cobalt polypyrrole structures are more stable than hydrated cobalt ions. We also performed free energy calculations for a few selected systems. The results (not shown) indicate that the entropy and enthalpy corrections for the respective systems are in the range of 0.13 to 0.35 eV, not high enough to significantly affect the calculated free energy changes, which remain below −2 eV.

Table 1. Optimized Structure of Model Cobalt Polypyrrole Systems

system	spin multiplicity	R_{Co-N} (Å) (average)	R_{Co-O} (Å) (average)	$R_{Co-N/O}$ (Å) (average)
A1	2	1.93	2.02	1.99
A2	2	2.00	2.34	2.23
B1	2	1.89	2.23	2.12
C1	2		1.93	1.93
average				2.07
experiment				2.07

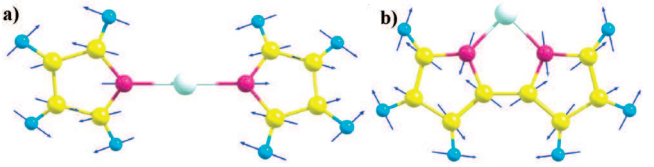

Figure 6. Vibrational mode corresponding to increased infrared absorption at 1071 cm^{-1} for structure A1 (a) and 1048 cm^{-1} for structure B1 (b). (Color: light blue − Co; pink − N; yellow − C; blue − H.).

Reversible Potential Calculations. To evaluate and understand reaction mechanism, one needs to know the oxidation state of cobalt at different potentials. To achieve this, we employed the reversible potential calculation methodology presented in computational section. We calculated the reversible potential of the model systems (Table 3). Based on the theoretical results, Co may exist in +3 or +2 oxidation states between 0.2 and 0.8 V vs RHE, i.e. in the potential range used in the previous experimental study.[35] The oxidation state depends on the metal coordination and is +2 for A2 and C1, +3 for B1, and +2 or +3 for A1. The redox potential calculated for the latter structure (*ca.* 0.34 V vs RHE) agrees reasonably well with that determined experimentally by Yuasa et al. for a Co(III)/Co(II) redox couple in their CoPPy catalyst (*ca.* 0.54 V vs RHE).[34] With knowledge of redox potential of these model systems, we can identify the state which initiates the oxygen adsorption process as discussed in the next section.

Reaction Mechanism Studies: Oxygen Adsorption Model. The slow ORR kinetics originates from the high strength of the O−O bond; the function of the catalyst is to facilitate the dissociation of that bond. The catalyst's ability to interact with oxygen and the degree of that interaction are essential for its activity in the oxygen reduction reaction. If the interaction between the catalyst and oxygen (the M−O interaction) is very weak, then the catalyst is likely to show no catalytic activity. However, too strong an interaction leads to the poisoning of the catalyst surface and renders it inactive (Sabatier's law[59]). There are three generally accepted types of interaction between transition metals and oxygen: side-on, end-on, and bridge (Figure 7).[60]

Yeager has proposed that the type of interaction between catalyst and oxygen dictates the oxygen reduction pathway and reduction products.[61] For side-on adsorption, more electrons are transferred to oxygen, which weakens the O−O bond to the extent that an O−O bond breaking becomes inevitable. Therefore, a four-electron (4e) reduction is likely to follow, resulting in water as a sole reaction product. Alternatively, the catalysts that

Table 2. Calculated reaction energies

Structure	System	Calculated ΔE (eV)
A1	PPy-CoPPy-$(H_2O)_4$	−2.55 (eq 12)
A2	PPy_3-Co-PPy_3 -$(H_2O)_4$	−2.89 (eq 12)
B1	Co-PPy_2-$(H_2O)_4$	−2.40 (eq 13)
C1	Co-$HPPy_3$-$(H_2O)_2(OH)_2$	−2.43 (eq 14)

Table 3. Calculated Co(III)/Co(II) reversible potential of the model systems

Model	Calculated reversible potential vs RHE (V)
A1	0.34
A2	0.91
B1	0.16
C1	1.17

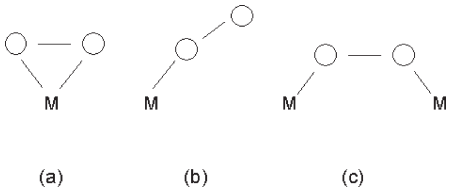

Figure 7. Illustration of oxygen adsorption configurations.

do not stretch the O−O bond to such extend as to break the bond can assist in a 2-electron (2e) reduction of oxygen to H_2O_2. The latter process may be followed by several electrochemical and/or chemical steps, eventually resulting in an indirect 4e reduction of oxygen to water.[62] In this work, we adopted Yeager's concept and used oxygen adsorption configuration as a base for deducing the reaction pathway, i.e., the side-on adsorption indicating a 4e pathway and the end-on adsorption attesting to either 2e or 4e pathways. On the basis of our current knowledge of Co-catalyzed oxygen reduction reaction, we further postulate that the end-on adsorption on Co leads to 2e products. In this work, we have calculated the end-on and side-on oxygen adsorption on model structures with either Co(II) or Co(III) as active centers.

As illustrated in Figure 5, cobalt is coordinated with polypyrrole and water ligands. With the presence of oxygen, the oxygen will replace water (see Figure 8) and be adsorbed on Co. For end-on adsorption, our work showed that one water molecule would be replaced. For side-on adsorption, as more space is required, two water molecules would be replaced. The energy change of oxygen adsorption to the catalyst is calculated using the following equation:

$$E_{\text{ads-O}_2} = E_{\text{catalyst-O}_2} + E_{\text{H}_2\text{O}} - E_{\text{catalyst}} - E_{\text{O}_2} \qquad (15)$$

where $E_{\text{catalyst-O2}}$, E_{H2O}, E_{catalyst}, and E_{O2} are energy of catalyst with oxygen adsorbed on, energy of water, energy of catalyst and energy of oxygen respectively. A negative adsorption energy value indicates an exothermic adsorption process. The calculation results are summarized in Table 4.

Several observations stem from the data in Table 4: (a) The end-on and side-on configurations are all stable, except for A1 with Co(III). (This result is quite different from those for Co porphyrin and phthalocyanine catalysts, in which cases the side-on configuration is not stable.)[41]; (b) among the active-site

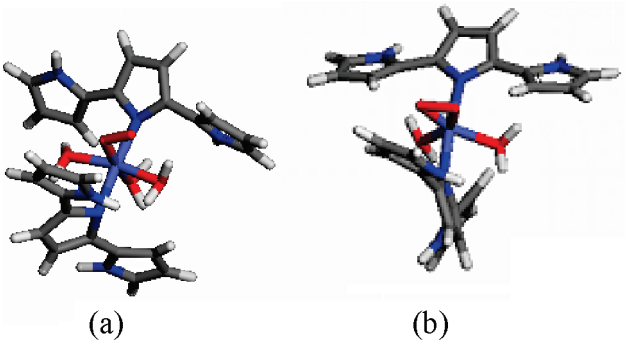

Figure 8. , Example of oxygen adsorption structures: (a) end-on adsorption on A2 structure; (b) side-on adsorption on A2 structure. (Color: light blue − Co; dark blue − N; red − O; gray − C; white − H.).

structures studied, the end-on adsorption is preferred on all instances, except A2; (c) in the case of structure A1, with Co(III) as an active center, the side-on adsorption is not stable and end-on adsorption is likely too weak for ORR catalysis.

Further examination of the side-on adsorption configuration reveals that the instability of that O_2 adsorption mode for cobalt porphyrins and phthalocyanines might be attributed to the planar structure of these systems. The plane defined by the Co center and four coordinated nitrogens cannot accommodate the side-on diatomic oxygen molecule. In order to allow for a stable interaction with a side-on O_2, cobalt needs to be out of the plane defined by the nitrogens.

The active centers and reaction mechanisms for possible oxygen configurations and adsorption energies are presented in Table 5. At a low potential, the active-site structure A1 with Co(II) active center is expected to support the 2e pathway. At a high electrode potential, the active-site structure A1 does not have catalytic activity as its ability to bind oxygen is very limited. The active-site structure A2, which involves two three-polypyrrole chains, should contribute mainly to the 4e pathway. While for active-site structure B1, the end-on and side-on adsorption energies are very similar; the structure will contribute equally to the 2e and 4e pathways. The active-site structure C1 will contribute mainly to the 2e pathway. On the basis of these results, at 0.3 V there are more 2e pathways than 4e pathways. At 0.6 V, the 2e pathways decrease due to the fact that at this potential Co(III) in the type A1 structure does not effectively catalyze the ORR. From these structure models, we can obtain the following qualitative analysis: at low potential there are more 2e pathways than that at high potential, hence more hydrogen peroxide yield and low electron transfer number at low potential. Although this analysis is based on the limited model structures, it is interesting to see that the trend is consistent with experimental observation. At 0.3 V, RRDE experiments give 88% hydrogen peroxide yield (the yield corresponding to an average transfer of 2.2 electrons per one O_2 molecule) while at 0.6 V, 68% peroxide yield (2.8 electrons per one O_2 molecule) (Figure 9).

A reduction peak potential of 0.44 V vs RHE[33] and a dominant two electron pathway for ORR on cobalt doped polypyrrole films was reported in another experimental study. The analysis presented above can also account for the observed such a two-electron reduction pathway.

We can further extend this analysis to heat-treated catalysts. In heat-treated systems, it is generally believed that a network is formed among active site and carbon.[63] Since A1 structure is a

Table 4. Calculated Oxygen Adsorption Energies

model/oxidation state	end-on adsorption energy (eV)	side-on adsorption energy (eV)
A1/Co(II)	−1.32	−1.12
A1/Co(III)	−0.25	0.18
A2/Co(II)	−0.38	−0.77
B1/Co(III)	−0.86	−0.76
C1/Co(II)	−0.93	−0.61

Table 5. Active Centers and Possible ORR Mechanism at Different Potentials

structure	active center	dominate ORR mechanism
	at 0.3 V vs RHE	
A1	Co(II)	2e
A2	Co(II)	4e
B1	Co(III)	2e, 4e
C1	Co(II)	2e
	at 0.6 V vs RHE	
A2	Co(II)	4e
B1	Co(III)	2e, 4e
C1	Co(II)	2e

one-unit isolated structure, the least networked structure. This isolated structure is unlikely to exist after the high-temperature treatment, which will lead to a reduction in the hydrogen peroxide yield in heat-treated catalysts. Such an H_2O_2 yield reduction was indeed experimentally observed in reported work.[35]

DISCUSSION

Theoretical simulation indicates that various active-site structures could contribute to the ORR activity of non-heat-treated Co-PPy catalysts, with both Co(III) and Co(II) playing the role of an active center, i.e., the center that initiates the interaction with O_2. In reality, given the fact that ORR involves electron transfer processes, both Co(III) and Co(II) play a role in the catalysis. The type A structure, where Co can exist in either +3 or +2 or both +3 and +2 oxidation states in the potential region of interest (Tables 4 and 5), can contribute to the observed potential dependence of the hydrogen peroxide generation rate. We therefore postulate that for untreated Co-PPy composites, the presence of the type A structure is likely. Also, experimental studies indicate that the cobalt to nitrogen ratio is about 1:2,[35] as expected for the type A structure.

Experiments have shown that the amount of peroxide production is potential dependent. Our theoretical calculations indicate that this may be related to the dependence of the active center formation on potential and its participation in different reaction pathways. The calculations thus imply that more than one active site contributes to the ORR activity observed with untreated cobalt-polypyrrole catalysts.

Another insight provided by the theory is that the side-on oxygen adsorption requires more space than the end-on adsorption. This may be one of the reasons why cobalt porphyrin and phthalocyanine systems cannot form stable side-on adducts. The destruction of the ordered structure of such a macrocyclic catalyst during the heat treatment is likely to increase the number of sites that facilitate the side-on oxygen adsorption and this lead to an increase in the number of electrons transferred in the ORR.

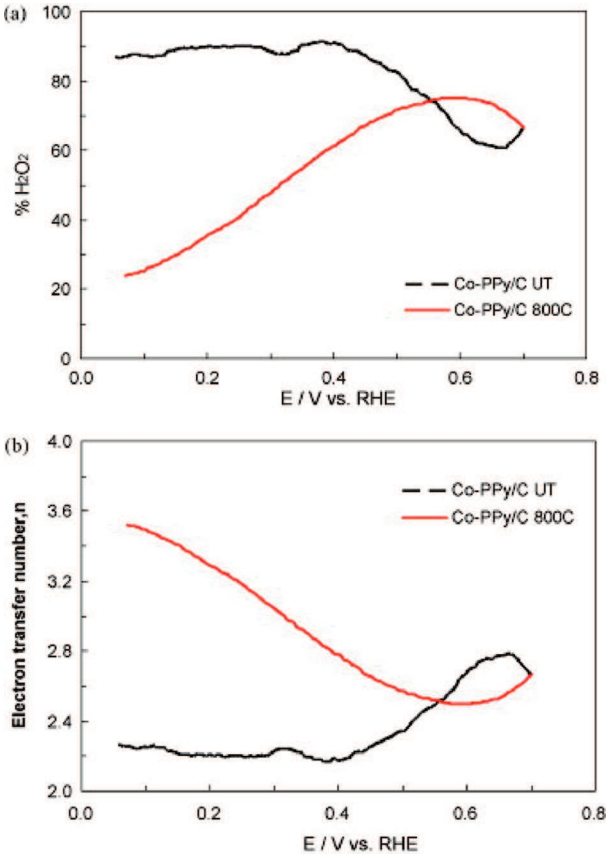

Figure 9. Experimental RRDE results for untreated (UT) and heat treated (800 °C) Co-PPy/C: (a) hydrogen peroxide yield; (b) electron transfer number as a function of electrode potential.[35].

CONCLUSIONS

In a theoretical study of the cobalt-polypyrrole ORR catalyst, we investigated four types of active-site structures and evaluated their stability, redox potential, and O_2 adsorption configuration. We also discussed possible reaction mechanisms. The computational results are compared with available experimental data such as FTIR, XRD, EXAFS, and CV. The results of the work were used for the interpretation of the experimental data obtained with the non heat-treated CoPPy catalyst system. The conclusions from this study can be summarized as follows:

(1) The active-site structure involving cobalt coordinated by four nitrogens in separate polypyrrole chains is not possible.

(2) A strong coordination bond can be formed between cobalt and a negatively charged (deprotonated) pyrrolic nitrogen but not between cobalt and neutral (protonated) pyrrolic nitrogen.

(3) There are many possible ORR active-site structures with significantly different redox potentials and oxygen binding energies. Both the redox potential and O_2 binding energy are greatly affected by the polypyrrole-chain size. Depending on active-site structure, both Co(III) and Co(II) could act as active centers.

(4) The cobalt-polypyrrole system can participate in the formation of stable oxygen adducts in both end-on and side-on configurations, which represents a notable difference between these catalysts and cobalt porphyrin and cobalt phthalocyanine systems.
(5) The type A1 structure is likely responsible for the potential dependence of hydrogen peroxide formation (the average number of electrons transferred in the ORR). A decrease in the H_2O_2 yield observed with heat-treated systems can possibly be linked to the disappearance of the type A1structure in the catalyst.
(6) A good correlation between experimental and calculated redox potentials was demonstrated with the modified redox potential calculation method.

Our work demonstrates that the structure of cobalt polypyrrole system is indeed very complex. With limited structure models, we can qualitatively explain the experimentally observed peroxide formation at different potentials. Further studies are required to get a complete review of the cobalt polypyrrole system.

AUTHOR INFORMATION

Corresponding Author
*E-mail: zheng.shi@nrc.gc.ca.

Present Addresses
[§]Oak Ridge National Laboratory, P.O. Box, 2008, Oak Ridge, TN 37831, United States.
[∥]SHOWA DENKO K. K. 1−1−1, Ohnodai, Midori-Ku, Chiba-Shi, Chiba 267−0056 Japan.

ACKNOWLEDGMENT

The authors would like to acknowledge financial support for this work from the National Research Council Canada Institute for Fuel Cell Innovation, Energy Efficiency and Renewable Energy Office of the U.S. DOE through Fuel Cell Technologies Program, and from Los Alamos National Laboratory through Laboratory-Directed Research and Development program (LDRD). M.W.B. would like to acknowledge the U.S. Department of Energy (DOE), Office of Basic Energy Sciences (OBES), Division of Materials Sciences and Engineering for support.

REFERENCES

(1) Dodelet, J. P. 3-Oxygen Reduction in PEM Fuel Cell Conditions: Heat-Treated Non-Precious Metal-N4Macrocycles and Beyond. In *N4-Macrocyclic Metal Complexes*; Zagal, J. H., Bedioui, F., Dedelet, J.-P., Eds.; Springer: New York, 2006; pp 83−147.
(2) From http://www.platinum.matthey.com.
(3) Bashyam, R.; Zelenay, P. A class of non-precious metal composite catalysts for fuel cells. *Nature* **2006**, *443* (7107), 63–66.
(4) Lefevre, M.; Proietti, E.; Jaouen, F.; Dodelet, J. P. Iron-Based Catalysts with Improved Oxygen Reduction Activity in Polymer Electrolyte Fuel Cells. *Science* **2009**, *324* (5923), 71–74.
(5) Zelenay, P. Advanced cathode catalysts. DOE 2010 Vehicle technology and hydrogen programs Annual Merit Review and Peer Evaluation Meeting, Washington, DC, 2010.
(6) http://www1.eere.energy.gov/hydrogenandfuelcells/mypp/pdfs/fuel_cells.pdf, Internet Communication 2007.
(7) Scherson, D. A.; Gupta, S. L.; Fierro, C.; Yeager, E. B.; Kordesch, M. E.; Eldridge, J.; Hoffman, R. W.; Blue, J. Cobalt tetramethoxyphenyl porphyrin—emission Mossbauer spectroscopy and O_2 reduction electrochemical studies. *Electrochim. Acta* **1983**, *28* (9), 1205–1209.
(8) Scherson, D.; Tanaka, A. A.; Gupta, S. L.; Tryk, D.; Fierro, C.; Holze, R.; Yeager, E. B.; Lattimer, R. P. Transition metal macrocycles supported on high area carbon: Pyrolysis—mass spectrometry studies. *Electrochim. Acta* **1986**, *31* (10), 1247–1258.
(9) Gupta, S.; Tryk, D.; Bae, I.; Aldred, W.; Yeager, E. Heat-treated polyacrylonitrile-based catalysts for oxygen electroreduction. *J. Appl. Electrochem.* **1989**, *19* (1), 19–27.
(10) van Veen, J. A. R.; Colijn, H. A.; Van Baar, J. F. On the effect of a heat treatment on the structure of carbon-supported metalloporphyrins and phthalocyanines. *Electrochim. Acta* **1988**, *33* (6), 801–804.
(11) Wiesener, K. N4-chelates as electrocatalysts for cathodic oxygen reduction. *Electrochim. Acta* **1986**, *31*, 1073–1078.
(12) Wiesener, K.; Ohms, D.; Neumann, V.; Franke, R. N4 macrocycles as electrocatalysts for the cathodic reduction of oxygen. *Mater. Chem. Phys.* **1989**, *22* (3−4), 457–475.
(13) Faubert, G.; Lalande, G.; Cote, R.; Guay, D.; Dodelet, J. P.; Weng, L. T.; Bertrand, P.; Denes, G. Heat-treated iron and cobalt tetraphenylporphyrins adsorbed on carbon black: Physical characterization and catalytic properties of these materials for the reduction of oxygen in polymer electrolyte fuel cells. *Electrochim. Acta* **1996**, *41* (10), 1689–1701.
(14) Jaouen, F.; Serventi, A. M.; Lefevre, M.; Dodelet, J. P.; Bertrand, P. Non-noble electrocatalysts for O_2 reduction: How does heat treatment affect their activity and structure? Part II. Structural changes observed by electron microscopy, raman, and mass spectroscopy. *J. Phys. Chem. C* **2007**, *111* (16), 5971–5976.
(15) Jaouen, F.; Dodelet, J. P. Average turn-over frequency of O_2 electro-reduction for Fe/N/C and Co/N/C catalysts in PEFCs. *Electrochim. Acta* **2007**, *52* (19), 5975–5984.
(16) Medard, C.; Lefevre, M.; Dodelet, J. P.; Jaouen, F.; Lindbergh, G. Oxygen reduction by Fe-based catalysts in PEM fuel cell conditions: Activity and selectivity of the catalysts obtained with two Fe precursors and various carbon supports. *Electrochim. Acta* **2006**, *51* (16), 3202–3213.
(17) Bonakdarpour, A.; Lefevre, M.; Yang, R.; Jaouen, F.; Dahn, T.; Dodelet, J. P.; Dahn, J. R. Impact of loading in RRDE experiments on Fe—N—C Catalysts: Two- or four-electron oxygen reduction?. *Electrochem. Solid-State Lett.* **2008**, *11* (6), B105–B108.
(18) Charreteur, F.; Jaouen, F.; Ruggeri, S.; Dodelet, J. P. Fe/N/C non-precious catalysts for PEM fuel cells: Influence of the structural parameters of pristine commercial carbon blacks on their activity for oxygen reduction. *Electrochim. Acta* **2008**, *53* (6), 2925–2938.
(19) Jaouen, F. ü. ü.; Dodelet, J. P. O_2 Reduction Mechanism on Non-Noble Metal Catalysts for PEM Fuel Cells. Part I: Experimental Rates of O_2 Electroreduction, H_2O_2 Electroreduction, and H_2O_2 Disproportionation. *J. Phys. Chem. C* **2009**, *113* (34), 15422–15432.
(20) Meng, H.; Jaouen, F.; Proietti, E.; Lefèvre, M.; Dodelet, J. P. pH-effect on oxygen reduction activity of Fe-based electro-catalysts. *Electrochem. Commun.* **2009**, *11* (10), 1986–1989.
(21) Jaouen, F.; Herranz, J.; Lefèvre, M.; Dodelet, J. P.; Kramm, U. I.; Herrmann, I.; Bogdanoff, P.; Maruyama, J.; Nagaoka, T.; Garsuch, A.; Dahn, J. R.; Olson, T.; Pylypenko, S.; Atanassov, P.; Ustinov, E. A. Cross-Laboratory Experimental Study of Non-Noble-Metal Electrocatalysts for the Oxygen Reduction Reaction. *ACS Appl. Mater. Interfaces* **2009**, *1* (8), 1623–1639.
(22) Herranz, J.; Lefèvre, M.; Dodelet, J. P. Metal-Precursor Adsorption Effects on Fe-Based Catalysts for Oxygen Reduction in PEM Fuel Cells. *J. Electrochem. Soc.* **2009**, *156* (5), B593–B601.
(23) Birry, L.; Zagal, J. H.; Dodelet, J. P. Does CO poison Fe-based catalysts for ORR?. *Electrochem. Commun.* **2010**, *12* (5), 628–631.
(24) Tributsch, H.; Koslowski, U. I.; Dorbandt, I. Experimental and theoretical modeling of Fe-, Co-, Cu-, Mn-based electrocatalysts for oxygen reduction. *Electrochim. Acta* **2008**, *53* (5), 2198–2209.
(25) Barazzouk, S.; Lefèvre, M.; Dodelet, J. P. Oxygen Reduction in PEM Fuel Cells: Fe-Based Electrocatalysts Made with High Surface Area Activated Carbon Supports. *J. Electrochem. Soc.* **2009**, *156* (12), B1466–B1474.
(26) Gong, K.; Du, F.; Xia, Z.; Durstock, M.; Dai, L. Nitrogen-Doped Carbon Nanotube Arrays with High Electrocatalytic Activity for Oxygen Reduction. *Science* **2009**, *323* (5915), 760–764.

(27) Anderson, A. B.; Sidik, R. A. Oxygen Electroreduction on Fe^{II} and Fe^{III} Coordinated to N_4 Chelates. Reversible Potentials for the Intermediate Steps from Quantum Theory. *J. Phys. Chem. B* **2004**, *108* (16), 5031–5035.

(28) Jain, M.; Chou, S.; Siedle, A. In Search for Structure of Active Site in Iron-Based Oxygen Reduction Electrocatalysts. *J. Phys. Chem. B* **2006**, *110* (9), 4179–4185.

(29) Vayner, E.; Anderson, A. B. Theoretical Predictions Concerning Oxygen Reduction on Nitrided Graphite Edges and a Cobalt Center Bonded to Them. *J. Phys. Chem. C* **2007**, *111* (26), 9330–9336.

(30) Titov, A.; Zapol, P.; Král, P.; Liu, D. J.; Iddir, H.; Baishya, K.; Curtiss, L. A. Catalytic Fe-*x*N Sites in Carbon Nanotubes. *J. Phys. Chem. C* **2009**, *113* (52), 21629–21634.

(31) Sidik, R. A.; Anderson, A. B.; Subramanian, N. P.; Kumaraguru, S. P.; Popov, B. N. O_2 Reduction on Graphite and Nitrogen-Doped Graphite: Experiment and Theory. *J. Phys. Chem. B* **2006**, *110* (4), 1787–1793.

(32) Ikeda, T.; Boero, M.; Huang, S. F.; Terakura, K.; Oshima, M.; Ozaki, J. i. Carbon Alloy Catalysts: Active Sites for Oxygen Reduction Reaction. *J. Phys. Chem. C* **2008**, *112* (38), 14706–14709.

(33) Ikeda, O.; Okabayashi, K.; Tamura, H. Electrocatalytic reduction of oxygen on cobalt-doped polypyrrole films. *Chem. Lett.* **1983**, 1821–1824.

(34) Yuasa, M.; Yamaguchi, A.; Itsuki, H.; Tanaka, K.; Yamamoto, M.; Oyaizu, K. Modifying Carbon Particles with Polypyrrole for Adsorption of Cobalt Ions As Electrocatatytic Site for Oxygen Reduction. *Chem. Mater.* **2005**, *17* (17), 4278–4281.

(35) Lee, K.; Zhang, L.; Liu, H.; Hui, R.; Shi, Z.; Zhang, J. Oxygen reduction reaction (ORR) catalyzed by carbon-supported cobalt polypyrrole (Co-PPy/C) electrocatalysts. *Electrochim. Acta* **2009**, *54* (20), 4704–4711.

(36) Delley, B. An all-electron numerical method for solving the local density functional for polyatomic molecules. *J. Chem. Phys.* **1990**, *92* (1), 508–517.

(37) Delley, B. From molecules to solids with the DMol[sup 3] approach. *J. Chem. Phys.* **2000**, *113* (18), 7756–7764.

(38) Vosko, S. J.; Wilk, L.; Nusair, M. Accurate spin-dependent electron liquid correlation energies for local spin density calculations: A critical analysis. *Can. J. Phys.* **1980**, *58*, 1200–1211.

(39) Becke, A. D. *J. Chem. Phys.* **1988**, *88*, 2547–2553.

(40) Perdew, J. P.; Wang, Y. *Phys. Rev. B* **1992**, *45*, 13244.

(41) Shi, Z.; Zhang, J. Density Functional Theory Study of Transitional Metal Macrocyclic Complexes' Dioxygen-Binding Abilities and Their Catalytic Activities toward Oxygen Reduction Reaction. *J. Phys. Chem. C* **2007**, *111* (19), 7084–7090.

(42) Norskov, J. K.; Rossmeisl, J.; Logadottir, A.; Lindqvist, L.; Kitchin, J. R.; Bligaard, T.; Jonsson, H. Origin of the Overpotential for Oxygen Reduction at a Fuel-Cell Cathode. *J. Phys. Chem. B* **2004**, *108* (46), 17886–17892.

(43) Karlberg, G. S.; Rossmeisl, J.; Norskov, J. K. Estimations of electric field effects on the oxygen reduction reaction based on the density functional theory. *Phys. Chem. Chem. Phys.* **2007**, *9* (37), 5158–5161.

(44) Bard, A. J.; Parsons, R.; Jordan, J. *Standard Potentials in Aqueous Solution*; Marcel Dekker, Inc.: New York and Basel, 1985.

(45) Hoselitz, K. *Ferromagenetic Properties of Metals and Alloys*; Clarendon Press: Oxford, 1952.

(46) Baker, J. M.; Bluck, L. J. C.; Cockayne, B.; MacEwen, W. R. Electron paramagnetic resonance of InP:Co. *J. Phys. C: Solid State Phys.* **1981**, *14*, 3953–3956.

(47) Kumar, N.; Sinha, K. P. Temperature dependent exchange narrowing of line width in EPR on interacting donors in germanium and silicon. *Z. Phys.* **1966**, *197*, 26–31.

(48) Martinez, W. M.; Thompson, T. T.; Smit, M. A. Characterization and Electrocatalytic Activity of Carbon-Supported Polypyrrole-Cobalt-Platinum Compounds. *Int. J. Electrochem. Sci.* **2010**, *5*, 931–943.

(49) Bernal, I.; Reisner, G. M.; Brunner, H.; Riepl, G. Optically active transition-metal compounds: XXII. Stereochemistry and crystal structure determination of $(\eta^5\text{-}C_5H_5)CoI(NC_4H_3C(R){=}N(S){-}CH(CH_3)\text{-}(C_6H_5))$ (R = H, CH_3). *J. Organomet. Chem.* **1985**, *284* (1), 115–128.

(50) Chlistunoff, J.; Zelenay, P. Semi-Empirical Modeling of Co-Polypyrrole Composites: Oxygen Reduction Reaction Catalysis. 213th Meeting of the Electrochemical Society, 2008, May 18 −22, Phoenix, AZ.

(51) Ortí, E.; Sánchez-Marín, J.; Tomás, F. Conformational behaviour of 2,2′-bipyrrole. *Theor. Chem. Acc.: Theory Comput. Modeling (Theor. Chim. Acta)* **1986**, *69* (1), 41–49.

(52) Bashyam, R.; Johnston, C. M.; Conradson, S. D.; Zelenay, P. Non-precious metal nanocomposite ORR catalysts: RRDE and single fuel cell studies. 212th meeting of the electrochemical society, 2007, October 7−12, Washington, DC, Abstract 583.

(53) *Gaussian 09*, version A. 02; Gaussian Inc.: Wallingford, CT: 2009.

(54) Dunning Jr.; T. H.; Hay, P. J. in *Modern Theoretical Chemistry*; Schaefer III, H. F., Ed.; Plenum: New York; 1976, Vol. 3, pp 1−28.

(55) Hay, P. J.; Wadt, W. R. Ab initio effective core potentials for molecular calculations. Potentials for the transition metal atoms Sc to Hg. *J. Chem. Phys.* **1985**, *82* (1), 270–283.

(56) Wadt, W. R.; Hay, P. J. Ab initio effective core potentials for molecular calculations. Potentials for main group elements Na to Bi. *J. Chem. Phys.* **1985**, *82* (1), 284–298.

(57) Hay, P. J.; Wadt, W. R. Ab initio effective core potentials for molecular calculations. Potentials for K to Au including the outermost core orbitals. *J. Chem. Phys.* **1985**, *82* (1), 299–310.

(58) Becke, A. D. Density-functional thermochemistry. III. The role of exact exchange. *J. Chem. Phys.* **1993**, *98* (7), 5648–5652.

(59) Sabatier, P. Hydrogenation and Dehydrogenation by Catalysis. *Ber. Dtsch. Chem. Ges.* **1911**, *44*, 1984–2001.

(60) Shi, Z.; Zhang, J.; Liu, Z. S.; Wang, H.; Wilkinson, D. P. Current status of ab initio quantum chemistry study for oxygen electroreduction on fuel cell catalysts. *Electrochim. Acta* **2006**, *51* (10), 1905–1916.

(61) Yeager, E. Dioxygen electrocatalysis: mechanisms in relation to catalyst structure. *J. Mol. Catal.* **1986**, *38* (1−2), 5–25.

(62) Adzic, R. Recent Advances in the Kinetics of Oxygen Reduction. In *Electrocatalysis*, Lipkowski, J., Ross, P. N., Eds.; Wiley-VCH: New York, 1998; pp 197−242.

(63) Lefevre, M.; Proietti, E.; Jaouen, F.; Dodelet, J. P. Iron-Based Catalysts with Improved Oxygen Reduction Activity in Polymer Electrolyte Fuel Cells. *Science* **2009**, *324*, 71–74.